

Model-Assisted Image-Guided Liver Surgery Using Sparse Intraoperative Data

Amber L. Simpson, Prashanth Dumpuri, William R. Jarnagin
and Michael I. Miga

Abstract This chapter examines the application of intraoperatively acquired sparse data to model-assisted image-guided liver surgery. The results suggest intraoperative deformation correction from computer models and sparse data to be considerable. This is an important step in the translation of image-guided surgery techniques to the abdomen. Moreover, the algorithms explored are a cost-effective solution that potentially improves the application of surgery, is widely adoptable, and is relatively easy to integrate into current surgical workflow practices. While continued investigation towards improvement is needed, these do represent beneficial advances that can affect the clinical application of surgery today.

1 Introduction

Worldwide, hepatocellular carcinoma (HCC) is the seventh most prevalent cancer, and is third among cancer-related deaths [113]. With respect to demographics, 80% of all HCCs occur in low-resource countries with the number of cases being

A. L. Simpson · M. I. Miga (✉)
Vanderbilt University, Nashville, TN, USA
e-mail: michael.miga@vanderbilt.edu

A. L. Simpson
e-mail: amber.simpson@vanderbilt.edu

P. Dumpuri
Pathfinder Therapeutics Inc., Nashville, TN, USA
e-mail: prashanthd@pathsurg.com

W. R. Jarnagin
Memorial Sloan Kettering Cancer Center, New York, NY, USA
e-mail: jarnagiw@mskcc.org

significantly larger as a percentage of liver cancers than in developed countries. In developed countries, using the United States as an example, metastatic liver tumors are far more frequent than HCC. Depending on the treatment center, metastatic liver tumors make up approximately 72% of malignant tumors in the liver with approximately 69% of metastases deriving from colorectal carcinoma (CRC) [2, 13]. Considering that more than 140,000 new cases of colorectal cancer will be diagnosed in a typical year [2], with approximately 60% [13] developing metastatic liver disease, the impact on the healthcare of developed countries is considerable. Globally, the numbers of liver cancers are rising considerably and the healthcare concerns are growing accordingly. For example, when comparing the number of new liver cancers and deaths in the year of 2002 to that of the year of 2008, an approximate 19.5% increase in new liver cancers and 16.4% increase in deaths has taken place [113]. These sobering numbers associated with primary and metastatic liver cancer are staggering and when considering their growth in the past decade, the ability to manage and treat liver cancer has worldwide impact.

1.1 Standard Treatment

In light of this growing health concern, resection is the only option that is often performed with curative intent. Unfortunately, the resection of liver tumors remains a specialized and highly complex procedure that requires consideration of many variables (e.g. vascular control, distribution of tumors within the liver, and adequate residual liver volume). While risky and resource intensive, hepatic resection is now commonly performed for an increasing number of indications. The excellent five year survival rate (the range is 44–50% with metastatic colorectal tumors, the most common [31] in the U.S.) make it the gold standard approach [50] to treating selected patients with primary and metastatic liver cancer [86], despite its complexity.

Interestingly, investigators are beginning to encourage the initial use of other treatments, usually systemic chemotherapy, not as curative measures but to facilitate surgical therapy. For example, in the case of inoperable colorectal liver metastases, Garcea et al. state that ‘the aim of treatment should be down-staging of metastases to achieve resectability’ [40]. While aggressive surgery is an effective primary treatment strategy, it also risks the result of injury to the liver parenchyma, which can impair normal regeneration and put patients at risk for post-operative liver failure [84]. Despite this, the literature advocates more aggressive hepatic resections [31, 55, 86]. In one study specifically grouping subjects according to extent of resection, five year survival rates rose from 38 to 45% with no increase in complication rate [86]. Unfortunately, the patient population eligible for resective therapy is limited. Based on one study involving 2400 subjects presenting with metastatic CRC, only 20% of patients were eligible for surgical resection [55] (these numbers do not reflect the 24,000 patients with primary intrahepatic malignant tumors [2]). This discrepancy may result from many factors, but is likely influenced by the magnitude and complexity of hepatic resections as they are currently performed.



Fig. 1 A patient undergoing a right lobectomy: the liver (*left*) prior to resection, (*middle*) after resection, and the resected lobe. Note the *white* towel placed in the cavity, demarcating the location of the lobe prior to resection (*middle*) and the white tumor visible in the resected mass (*right*). In this case, the right hepatic artery extends centrally into the mass and touches the right hepatic vein and right portal vein

1.2 Clinical Barriers

Briefly described here, in an open hepatic resection procedure, a large incision through the abdomen is created to expose the anterior surface of the liver. Either wedge or anatomical liver resections are performed to remove one or more hepatic tumors. In wedge resections, the tumor and a 2–3 cm surrounding region of the liver is removed, while in anatomical resection, one or more segments of the liver is removed, based on the vascular anatomy. Each of the eight segments of the liver is supplied by its own portal venous and hepatic arterial pedicle [41]. A right lobectomy in which the portal and hepatic vein was entwined with the tumor is shown in Fig. 1.

Typically, a segmental hepatectomy, i.e. segmentectomy (separation along segment-based boundaries), is preferred to lobectomies or non-anatomic wedge resections. Segmentectomies preserve more tissue and are identifiable by liver color changes resulting from vascular in-flow occlusion. In the case of wedge resections, while they may preserve tissue, traction and bleeding can compromise the final resection margin which has dramatic effects on outcome [31]. More specifically, five year survival rates in patients with negative margins of less than 1 cm range from 18 to 26%, which is significantly worse than the 44 to 50% survival rate seen in patients with negative margins greater than 1 cm. In further comparing wedge versus segmental resection, in one study with over 260 patients, the rate of positive margins present following wedge removal was eight times higher than with segmentectomy [31].

The choice seems clear; however, as more liver is removed in a multi-segment or lobectomy procedure, complication rates increase. While liver resection has shown promising survival rates and a perioperative mortality rate of less than 5%, a significant increase in postoperative morbidity due to hepatic dysfunction and infection has also been reported, even by specialized centers [51, 65]. In one recent study, postoperative complications doubled when comparing major to minor hepatectomy procedures [16]. In a related study of over 100 patients that studied

hepatic dysfunction and infection after major liver surgery, Schindl et al. [99] used a regression analysis to demonstrate that dysfunction increases significantly when the relative residual liver volume (RLV) was below 26.6%. The authors believe that calculating a specific percentage of RLV before major liver surgery from a virtual resection on segmented computed tomography (CT) scans provided useful information for planning hepatic surgery.

It is clear that a detailed understanding of the liver anatomy and its geometry is used when conducting these complex procedures. With the realization that five year survival rates can double with well executed procedures, understanding the relationship between anatomic resection boundaries and tumors is imperative. However, aggressiveness must be tempered with the realization that unnecessary resection elevates complication rates. Going further, the recognition that preoperative plans estimating RLV based on resection information are valuable when considering that the postoperative complication rate is important for successful surgical outcome.

1.3 Surgical Guidance

With this backdrop, the translation of preoperative surgical planning coupled with accurate image-guided surgical therapy for open abdominal procedures would undoubtedly be a valuable tool for breaking down these surgical barriers and increasing the possibility of favorable outcomes for more patients undergoing this aggressive and complex procedure. Currently, there is active research and development in the area commonly referred to as image-guided liver surgery. For example, augmented reality systems are being developed that merge the real surgical field containing the liver within a virtual scene [45, 83, 107]. These works detail several hurdles to overcome, including the development of an accurate registration technique to map virtual to real space, one of the most difficult steps in image-guided surgery. Several groups are working on registration problems associated with liver surgery to include methods to determine the deformation and respiration movement of the liver during surgery which is critical for accurate mapping between physical and image space [11, 52, 81, 111]. Other laboratories are looking at robotic applications towards liver ablation and radiosurgery therapies [1, 89, 95, 104]. In addition, the value of intraoperative ultrasound has been recognized and several groups have been developing techniques to map preoperatively acquired liver magnetic resonance (MR) and CT images to ultrasound images [6, 7, 12, 23].

While strides in translating image-guidance technology to the abdomen have been made, there are still considerable challenges. In quantitative studies using intraoperative computed tomography, the presence of confounding deformations has been shown to compromise tradition organ-based image-guided liver navigation [47]. The work by Lange et al. [60–62] is looking at a CT-to-ultrasound (US) vessel based non-rigid registration system for providing the link between

image and physical space within the presence of deformation. While the three reported cases performed well, the likelihood of this approach working within the confines of OR workflow is limited. More specifically, while significant structures such as the tumor or the posterior side of the liver are easily recognized intraoperatively, distinct vasculature landmarks will likely take significantly longer. The automatic reconstruction of 3D objects as well as automatic segmentation in ultrasound is still a very difficult task. In addition, their method requires the identification of as many bifurcations as possible in the spatial neighborhood of the tumor using tracked ultrasound and then the determination of corresponding bifurcations within the CT. While the subsurface information would be valuable for non-rigid correction, the likelihood of misidentification in this highly vascularized organ is high, and the encumbrance could challenge adoption. Others have pursued intraoperative imaging solutions within primarily the ultrasound domain with more limited developments within the MR environment [7, 24, 28, 32, 44, 47, 57, 69, 73, 80, 108]. Another possibility is to acquire information regarding the exposed surfaces (either in open or minimally invasive) and then couple this acquired data to computer models to constrain volumetric deformation fields [19, 20, 26, 33]. This approach is highly robust with respect to surgical workflow as it can augment existing guidance systems quite easily.

Regardless of realization, there is ample evidence that improved visualization as provided by image-guidance for abdominal procedures is critical. Given the wealth of data taken preoperatively, the ability to align that data with the deforming organ intraoperatively is a barrier that needs to be overcome. Organ presentation, whether open or laparoscopic, requires that intraoperative collected data be used to register all preoperative data. Each solution proposed represents a balance between accuracy and utility and serves as constraints to data acquisition and guidance procedure execution. These constraints are the foundation of the *sparse data extrapolation problem*. More specifically, the problem of extrapolating cost-effective relevant patient information from distinctly finite or sparse data while balancing the competing goals between workflow and engineering design, and between application and accuracy is the *sparse data extrapolation problem* [77].

1.4 Compensating for Intraoperative Deformation

While intraoperative volumetric imaging as provided by magnetic resonance [10, 85] or X-ray computed tomography [47] are compelling technologies for the monitoring of intraoperative changes to soft-tissue, it does not represent a solution that is economically scalable to many medical centers, is very difficult to adapt to all clinical presentations for surgery, and incurs ionizing radiation in the latter. As described earlier, open abdominal surgery requires a level of patient access that is somewhat incompatible with these technologies. In addition, while providing differing degrees of soft-tissue contrast, these modalities still serve as primarily a tool to monitor anatomical changes only. The wealth of preoperative data

(e.g. single proton emission computed tomography, positron emitted tomography, diffusion MR imaging, MR/CT angiographic data, functional MR, MR elastography, etc.) cannot possibly be intraoperatively acquired for update during surgery, i.e. the ability to leverage the considerable battery of imaging techniques provided by MR and CT technology largely remains untapped intraoperatively due to the constraints of the OR environment. As a result, the need to align preoperative data to the intraoperative patient state is a persistent need.

While non-rigid image registration algorithms for image-to-image alignment abound in the literature to include numerous texts, the registration of preoperative to the intraoperative environment is more limited due to the extensive changes in the target domain [96]. These approaches predominantly fall into two categories data-rich, and sparse-data frameworks. An example of the former is that demonstrated by Clatz et al. [25] where a biomechanical model is used to constrain the deformation field produced by an iterative regularized least squares minimization process driven by a block-matching framework. The approach is driven by data-rich intraoperative MR and in a six patient preliminary study demonstrated an ability to correct for 50–90% of deformations with an average correction of approximately 73% across the cases. This work was later used to register functional and diffusion tensor magnetic resonance imaging to the intraoperative state [3] as well as further developments towards the resection environment [110]. This work is a good example of the use of intraoperative imaging as a solution for intraoperative correction. Interestingly, the second approach, whereby computer models are driven by sparsely available intraoperative data, has not shown a great deal of difference in results from the data-rich presentation. In recent reports, methods driven by ultrasound partial volume, stereo-pair microscope surface data, and/or organ surface laser range scan data have produced similar fidelity [22, 34, 46, 53, 70, 106, 109]. The reason for this non-intuitive similarity is due to the extent of change in a resection environment, i.e. there is such a significant change in the acquired images from the pre- to the intraoperative state due to tissue removal that it significantly challenges the data-rich realization. While interesting, both of these examples represent work within the neurosurgical environment which is where deformation correction needs began for image-guided surgery.

Within abdominal applications, some work has been forthcoming but the guidance environment is very different from its neurosurgical counterpart. The setting for image-guided liver surgery holds many unique challenges. For example, organ presentation often involves separation from the surrounding ligamenture and far-more mobilization. Once presented, the organ is then stabilized, i.e. *packed*, in a state which often produces organ deformation when compared to its preoperative CT images. Often, these actions are taken all before one can acquire data regarding shape change. In addition, diaphragmatic movement can cause shift in the organ that typically cause large semi-rigid translations of the organ (can usually be minimized with apneic periods). While these are considerable obstacles, fortunately, the robust physiological constitution of the liver allows for significantly larger resection margins (typically 1 cm into healthy tissue) which does reduce the accuracy requirements for successful use of guidance technology.

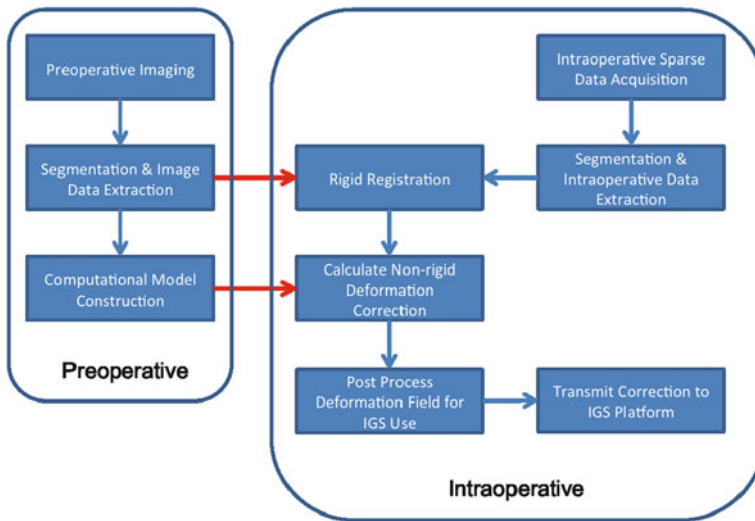


Fig. 2 Typical workflow for intraoperative deformation correction

Similar to the neurosurgical environment, while some intraoperative imaging solutions have been proposed [5, 47, 61, 73, 74], the workflow requirements have inhibited much of the tomographic work, and with respect to ultrasound imaging, while amenable to the workflow, it too has struggled with respect to the integration of preoperative imaging data and its use in intraoperative monitoring roles.

In this chapter, work towards a deformation correction framework will be presented and some preliminary results will be provided. The solutions presented typically have an implementation that reflects Fig. 2. The preoperative workflow reflects imaging, segmentation and data feature extraction, and then model building activities. Within the intraoperative environment, data regarding the target of interest is acquired, a rigid alignment process is executed, that alignment is then adjusted non-rigidly, and an update to the guidance system is provided.

2 Preoperative Tasks

A crucial step in any image-guided surgery application is the separation of the anatomy of interest from the surrounding tissues such that a three-dimensional patient-specific model can be constructed. The surgeon uses this model to create a preoperative plan in which the desired resection lines are defined and executed in the operating room. An accurate preoperative model is also necessary for defining boundary conditions in the finite-element model.

2.1 Image Segmentation and Planning

In CT images of the liver, the segmentation process is complicated because the intensity values in tumors and surrounding organs are similar to the liver which makes discerning the extents of the organ difficult [112]. In an elaborate study, across several research groups, Heimann et al. [112] evaluated the efficacy of semi-automatic and automatic liver segmentation methods on a series of clinical data sets. The methods included statistical shape models, atlas registration, level-sets, graph-cuts, and rule-based systems. The results showed that in general, methods that use some interaction have more consistent segmentations.

Scout Liver (Pathfinder Therapeutics Inc., Nashville, TN, USA), MeVisLab (MeVis Medical Solutions, Bremen, Germany), Myrian (Intrasense, Montpellier, France), and mint Liver (Mint Medical, Heidelberg, Germany) are amongst the handful of commercially available planners that provide segmentation of structures of interest in the liver. In addition to being an end-user application, MeVisLab¹ is also a closed source rapid application development tool that facilitates integration of image processing algorithms. 3D Slicer,² Seg3D,³ Caret,⁴ and ITK-SNAP⁵ are open-source applications which offer manual and semi-automatic segmentation tools. Osirix⁶ and AMIRA⁷ are closed source applications with integrated semi-automatic segmentation and visualization tools.

The segmentation method used by Scout Liver⁸ is based on a level set approach proposed by Dawant et al. [30, 49]. The method takes 5–15 min to run, and then up to 15 min of user interaction after the segmentation. This method has been evaluated at the Catholic University of Louvain in Belgium. The study aimed at comparing the accuracy and repeatability of the method with those of manual segmentation for determining liver volume from MR images of living liver transplant donors. The key findings were that (1) mean interaction time was reduced from 25 min with manual segmentation to 5 min for the semi-automatic method; (2) differences between the actual volume and the estimated volume ranged from −223 to +123 mL for manual segmentation and from −124 to +86 mL with the method; (3) semi-automatic segmentation improved organ weight estimation in 15 out of 18 cases; and, (4) inter- and intraobserver repeatability (reliability) was improved using the semi-automatic method [49]. Figure 3 shows a screen capture of the Scout Liver planning system used in a clinical evaluation.

¹ <http://www.mevislab.de/>

² <http://www.slicer.org/>

³ <http://www.sci.utah.edu/cibc/software>

⁴ http://brainvis.wustl.edu/wiki/index.php/Main_Page

⁵ <http://www.itksnap.org/>

⁶ <http://www.osirix-viewer.com/>

⁷ <http://www.amira.com/>

⁸ <http://www.pathsurg.com/>

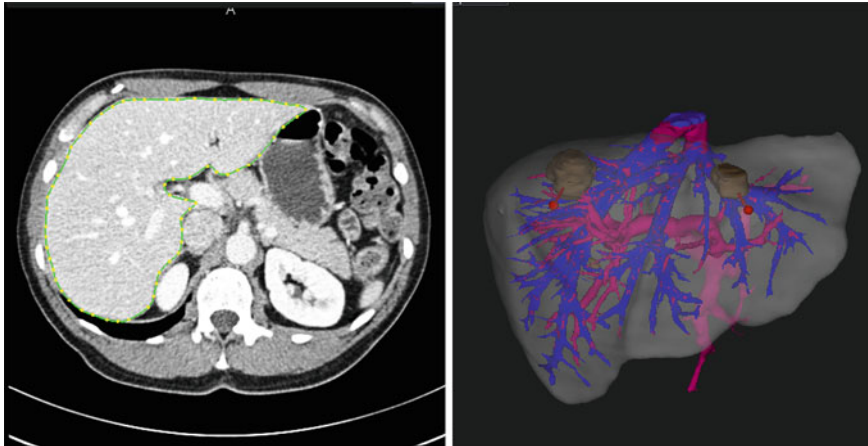


Fig. 3 Scout Liver preoperative planning software (Pathfinder Therapeutics Inc.) in use at Memorial Sloan-Kettering Cancer Center. (*left*) A green spline demarcates the liver boundary. (*right*) Preoperative plan of the liver including the tumor (*dark gray*), ablation path (*red*), portal vein (*magenta*), and hepatic vein (*blue*)

MeVisLab is a commercial system which consists of a set of tools for preoperative planning that allows a surgeon to explore the relationship between the intrahepatic vessels and tumors in a 3D surface representation of the liver [37, 59, 101]. Liver vessels are segmented from CT volumes using a refined region growing algorithm and then visualized by fitting graphics primitives along the skeleton lines. The user can choose arbitrary viewing directions, colors and transparency values and design individual visualizations. Given this wealth of 3D information, the user can then attempt resection strategies to estimate the consequences of a surgical intervention. In a study by Li et al. [66], a 94.6% overlap of the liver segmented with Scout and MeVisLab was found.

Myrian XP Liver⁹ is a pre-surgical planner for measuring liver volume, segmentation of hepatic and portal veins, parenchyma and lesions, and planning of surgical cutting planes. The software has been used for segmenting adrenal glands [87], calculating liver resection volume [92], and lung volume measurements [36]; however, the specifics of the segmentation algorithm are not reported. Mint Liver¹⁰ is a surgical planner built on the open-source Medical Imaging Toolkit in collaboration with the German Cancer Research Center (Heidelberg, Germany).

Several studies have shown that using three-dimensional models to plan liver surgery improves the efficiency and accuracy of resection margins [42, 56, 58, 59, 94]. The preoperative estimation of partial and total liver volumes is necessary for assessing the risk of organ failure [94]. In addition to identifying and segmenting the

⁹ http://www.intrasense.fr/pages/eng/media/Myrian_XPLiver.pdf

¹⁰ <http://www.mint-medical.de/productssolutions/mintliver/mintliver/>

liver and tumor tissue, planners also segment the liver vasculature and construct three-dimensional models of the hepatic and portal vessel structures [42, 101].

Some commercial systems such as Scout Liver, MeVisLab, and mint Liver also let the surgeon delineate resection lines and ablation paths on three-dimensional liver models. These provide useful information such as functional liver volume, remnant liver volume (volume of liver remaining after resection) and also help the surgeon estimate the consequences of surgical intervention by avoiding vessels. As discussed in the previous section, the liver deforms during surgery; hence, these preoperative plans should be used with caution in the operating room as the intraoperative presentation of the organ is significantly different to the preoperative models and images.

2.2 Surface Model Smoothing and Parameterization

While the above references speak to the process of segmentation, and the visualization of structure for image-guided surgery purposes, it does not really address the next step in model-based correction frameworks, i.e. the generation of the computation model for execution of finite element techniques. Using the segmented images, 3D surfaces can be tessellated using methods such as the Marching Cubes algorithm [68] which can generate a fitted liver surface. Once complete, a smoothed parametric representation of the marching cubes surface can be generated using tools such as the FastRBF Toolbox (Farfield Technologies, Christchurch, New Zealand). This surface will consist of connected triangles and can be used for image-to-physical surface registration. Once complete, a tetrahedral mesh generator [105] is to generate the 3D volumetric tetrahedral mesh which is required by the finite-element model. In the realization shown here, the domains were represented by elastic systems with tetrahedral elements. While these may not be the optimal element or even model choice for liver, we have found that with displacement-based boundary conditions and elastic properties that are moderately incompressible (i.e. Poisson's ratio of 0.45), the results add value to guidance systems and are tractable for real-time guidance applications.

3 Intraoperative Tasks

The strategy of augmenting existing image guidance with deformation correction (as depicted in Fig. 2) relies on acquiring sparse intraoperative data through surface or subsurface characterization which is described in Sect. 3.1. In the paradigm of model-assisted image-guided surgery described here, these acquisition methods would be low cost (with less resolution), thus facilitating wide-spread adoption. For completeness, intraoperative CT and MR are addressed in the context of liver surgery; however, there is little need to provide guidance system updates from

finite-element models in the presence of rich intraoperative images. The alignment (or *registration*) of intraoperative data with preoperative images remains a challenging task in image-guided surgery. [Section 3.2](#) compares registration methods specifically developed for the unique challenges of liver surgery and [Sect. 3.3](#) describes deformation correction provided by finite-element models. [Section 3.4](#) details the final task in model-assisted image-guided surgery, to propagate the deformation correction, computed by the model, to the guidance display for clinical interrogation.

3.1 Surface and Subsurface Characterization

Three low-cost acquisition methods used for initializing finite element models are described: hand swabbing, laser range scanning, and conoscopic holography. Ultrasound, intraoperative CT and MR, and Fluoroscopy are means of acquiring subsurface information.

3.1.1 Hand Swabbing

Swabbing the anatomy with a tracked stylus is a method of acquiring surface information intraoperatively. The advantages of this technique are that the surgeon has familiarity with the tool, line-of-sight of the stylus tip is not necessary, and the tool already exists in the image-guided surgery operative setup so additional equipment is unnecessary. In delicate structures such as the brain, it is impossible to directly touch the soft tissue. Collecting patient data in this way makes sense for anatomical structures that do not deform such as bone [72] and for initializing registrations involving the liver [26]. However, the fidelity of these registrations is compromised due to displacements in the soft tissue from contact force with the stylus or from the stylus losing contact with the surface. The deleterious effects of hand swabbing on registration accuracy have been studied [21, 75]. Two examples of hand swabbing are shown in [Fig. 4](#). In both examples, point data acquired by hand swabbing a rubber liver phantom was registered to a 3D model generated from preoperative CT data. The target registration error (TRE) was computed for each point in the preoperative model compared to a ground truth estimate. Indeed, it is straight forward to generate good and bad examples of hand swabbing acquisition on the same anatomy.

3.1.2 Laser Range Scanning

Laser range scanning (LRS) uses the principle of triangulation to determine the position of three-dimensional points in space [4]. A laser light is emitted from the scanner and strikes the surface. The reflected light is received by a charge-coupled

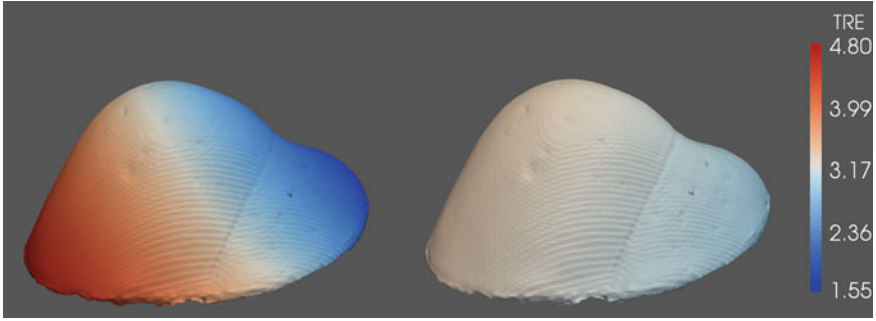


Fig. 4 The effect of hand swabbing liver phantom surfaces on registration error for two data collections. In this example, TRE is computed for each element in the preoperative mesh and reported in millimeters

device (CCD) camera, and based on the reflected light and the known trigonometric relationship between the laser emitter and the camera, the three-dimensional location can be computed. The CCD also captures a standard digital image that can be used to texture map the point cloud. The texture information provides valuable information for segmenting the organ as well as for finding salient features on the organ for the purposes of image-to-physical registration [102]. Figure 5 is an example of an LRS acquired intraoperatively of a patient undergoing hepatectomy. The field of view of the LRS, segmented geometric point cloud, and textured point cloud is shown.

By attaching optical tracking targets, the position and orientation of the scanner with respect to the patient can be determined such that all scans are in the same coordinate space which facilitates quantifying deformation from scan to scan. In laboratory studies of the LRS designed in conjunction with Pathfinder Therapeutics Inc. (Nashville, TN, USA), the geometric scanner accuracy mean error is 0.37 ± 0.40 mm [93]. When the LRS is tracked without wires (passive optical tracking) from different locations, the mean error is 1.49 ± 0.50 mm. The tracking accuracy of the previous generations of LRS was found to be 1.0 ± 0.5 mm [102] and 1.4 ± 0.8 mm [21] with wires (active optical tracking).

3.1.3 Conoscopic Holography

Conoscopic holography is a distance measurement technique originally reported by Sirat and Psaltis [103] based on analyzing constructive and destructive interference patterns between emitted and reflected laser light. The conoprobe emits a cone of laser light (solid angle) rather than relying on the less accurate method of triangulation used by laser-range scanning. Though conoscopic holography has been traditionally used for measuring distances in industrial quality control, recent techniques have been developed for non-contact surface acquisition that can be deployed through a laparoscopic port [64]. In this preliminary study, the

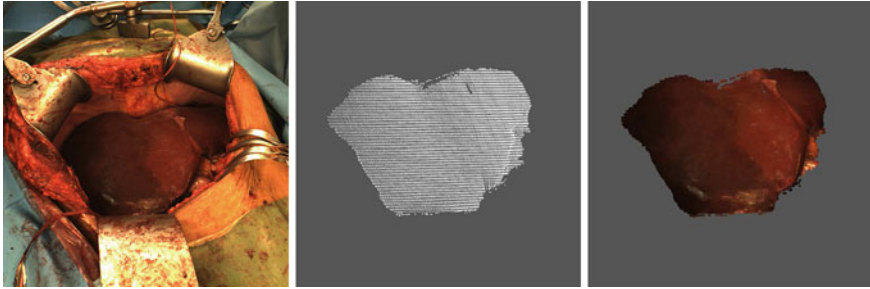


Fig. 5 (*left*) Digital image taken of the liver anatomy from the range scanner; (*middle*) point cloud acquired from laser-range scanner; and (*right*) point cloud with addition of texture information from laser-range scanner

Conoprobe Mark 3 (Optimet Metrology Ltd., Jerusalem, Israel) was combined with optical tracking technology such that a three-dimensional surface description of anatomy was obtained. The conoprobe reports the distance and direction of the laser source to the laser point on the surface. A calibration procedure establishes the transformation of the conoprobe points into the coordinate system of the optical tracking system. Figure 6 shows the conoprobe and conoprobe points rendered on the surface of a liver phantom. In this example, the tracked conoprobe is registered in real time, as data is collected from the conoprobe.

In a laboratory study of the tracked conoprobe, the observed root-mean-squared error was 0.58 mm. In another study, the effects of contact and non-contact surface acquisition techniques on TRE were investigated for soft tissue. A comparison of image-to-physical registrations using three different methods of organ spatial digitization: (1) a tracked laser range scanner, (2) a tracked pointer, and (3) a tracked conoprobe demonstrated that the conoprobe was more accurate with respect to TRE than either the LRS or tracked pointer. A comparison of the three acquisition methods with respect to TRE are shown in Fig. 7.

3.1.4 Ultrasound

Ultrasound is a valuable intraoperative imaging modality due to its low cost, pervasive use in operating rooms, and safety; however, in general, ultrasound images are noisy due to speckle and geometric distortion and can be difficult to interpret. It can be challenging to acquire high-resolution ultrasound images due to patient positioning, surgical access, and interference artifacts from surgical tools in the surgical field. Evidence suggests that ultrasound is a viable tool in liver surgery because vessel and tumor boundaries are visible in this imaging modality in both laparoscopic [54] and open surgeries [9]. Ultrasound is routinely used to locate tumors and guide liver resection as well as ablative technology [47]. The efficacy of image-guided liver surgery techniques using ultrasound has been studied for

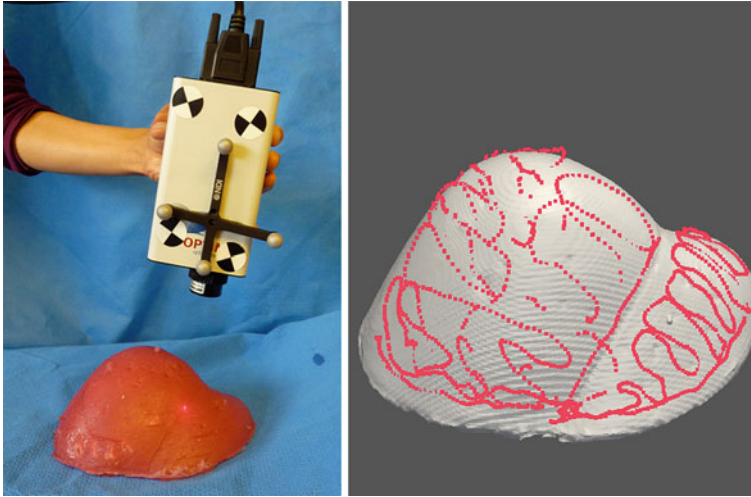


Fig. 6 (left) Conoprobe Mark 3 with NDI passive tracking markers. (right) Conoprobe points (rendered in red) collected on the surface of a liver phantom and registered to a preoperative model from CT

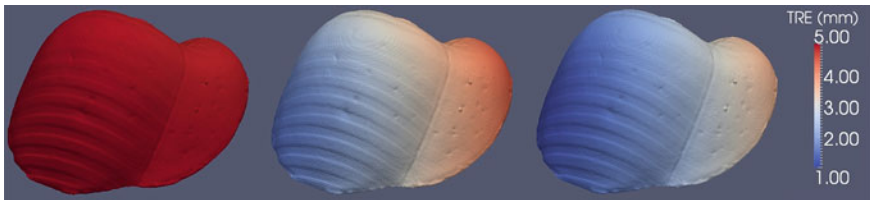
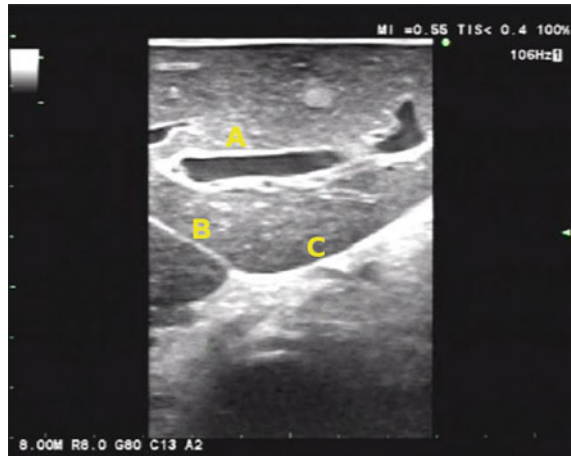


Fig. 7 A comparison of TREs computed for each element in the preoperative mesh for one (left) hand swabbing, (middle) LRS, and conoprobe acquisition. TRE increases from blue to white to red

phantom [6, 82], porcine [48], and human [7] images. Lange et al. [60–62] proposed a CT to US vessel-based non-rigid registration system where corresponding landmarks (typically vessel bifurcations) are identified. Automatic vessel segmentation has not been achieved in US [61] because of the challenge of localizing the extents of vasculature in images which is illustrated in Fig. 8.

The improved resolution of ultrasound images coupled with the low cost of the systems make ultrasound a good candidate for providing displacements to finite-elements models and establishing boundary conditions. At the time of writing, existing literature does not address this specific problem for the liver; however, techniques have been proposed for the neurosurgical domain.

Fig. 8 Ultrasound image collected during liver surgery at Memorial Sloan-Kettering Cancer Center; (A) left portal vein, (B) division between the caudate and left lobe, and (C) posterior edge of left lobe, designated



3.1.5 Intraoperative CT and MR

Interventional CT and MR are imaging modalities used for compensating for intraoperative soft tissue deformation. Both require a dedicated imaging device and a radiologist present for interpreting images [18]. As such, these modalities are not economically scalable to many medical centers. Non-metallic tools are required when working in the magnetic field of most MR units and the patient and surgical staff are exposed to ionizing radiation in the case of CT. Soft tissue deformation during liver resection has been documented with CT and has demonstrated significant effects [47]. Intraoperative MR has been studied with respect to ablative techniques [73, 74].

3.1.6 Fluoroscopy

Fluoroscopy is one of the most widely used interventional imaging modalities and as such could provide meaningful initial intraoperative displacements for use in finite-element modeling. Fluoroscopic images provide poor tissue contrast, subject the patient and surgical staff to ionizing radiation, and require 3D reconstruction. Newer 3D fluoroscopic systems are capable of reconstructing 3D images with reasonable speed and accuracy.

3.2 Registration

Integral to the display of preoperative patient images superimposed with intraoperatively acquired data, is the ability to align the preoperative images with the physical patient within the operating room. Without this, providing reliable guidance information to surgeons and pertinent surface displacement data for

deformation correction algorithms would be impossible. In previous work, image-to-physical space registration was performed using a traditional iterative closest point (ICP) algorithm [8] between the preoperative CT liver surface and an intraoperatively acquired point cloud of the liver surface provided by LRS [19–21]. This more conventional method can still be compromised by poor initial pose estimation as well as tissue deformation due to the laparotomy and liver mobilization performed prior to tumor resection.

To increase registration robustness for use in image-guided liver surgery, and as a good initial pose for deformation correction algorithms, an approach using weighted salient anatomical features identifiable in both the preoperative image set and intraoperative liver surface data was developed [26]. The algorithm is an ICP variant. Robustness studies were performed using both phantom and clinical data under conditions of varying initial pose. The results suggest that the proposed weighted patch registration algorithm is significantly better than traditional point-based and ICP. Figure 9 illustrates the steady improvement in results using our salient feature-based registration on a sample clinical case. A series of quantitative phantom experiments was also conducted. In these experiments, surface and subsurface targets were implanted to generate quantitative estimates of TRE [35]. Under conditions of modest and severe misalignment, salient feature ICP outperformed traditional ICP in all trials. When the alignment was successful, both methods produced an average residual closest point distance of approximately 0.6 ± 0.1 mm, with a TRE of 2.8 ± 0.3 mm. On patient data, the root mean square (RMS) error for salient-feature ICP was 3.7 ± 0.05 mm.

Penney et al. [90] developed a technique to map preoperatively acquired liver MR images to ultrasound images, by picking an initial point in each modality and computing vessel probability maps for registration. When compared with ‘bronze standard’ registration, the RMS target registration error improved from 15.4 to 4.3 mm using this technique. Peterhans et al. studied the effect of designating landmarks for registration and finding correspondence using Horn’s method [91]. The reported RMS landmark registration errors was less than 10 mm on clinical data. Lange et al. [61] propose CT-to-ultrasound vessel-based non-rigid registration system for providing the link between image and physical space. The method was tested on three clinical cases and required the identification of as many bifurcations as possible with tracked ultrasound and then the determination of corresponding bifurcations within the CT. The mean distance between corresponding points after rigid registration were in the range 4.4–4.7 mm and improved to 2.6–4.9 mm after non-rigid registration using thin-plate splines.

3.3 Deformation Correction Using Finite Elements

In the previous sections, the process of segmentation, model construction (geometry only), intraoperative data acquisition, and initial rigid registration were covered. In addition to building digital representations of the anatomy, one aspect

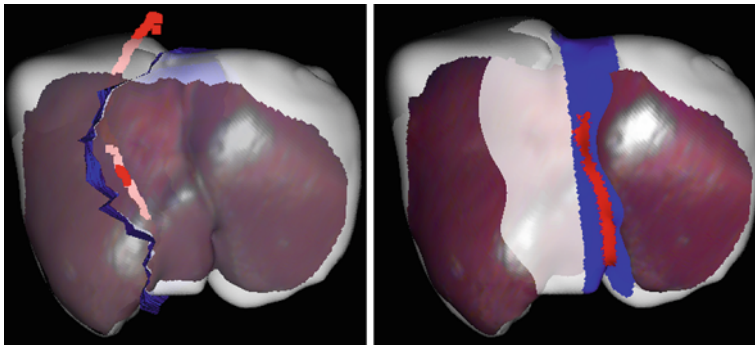


Fig. 9 Example of the misalignment of the intraoperative liver surface (*red*) and the preoperative image (*white*) after registration with ICP (*left*) and salient-feature ICP (*right*). Note the alignment of the preoperative falciform ligament (*blue*) and intraoperatively collected falciform ligament (*red*) is much better with salient-feature ICP (*right*)

that is common to many of the data-rich or sparse-data non-rigid alignment realizations is the utilization of biomechanical models to constrain the solution space to realistic deformation predictions. The classic partial differential equation that represents a state of static mechanical equilibrium is,

$$\nabla \cdot \sigma = 0 \quad (1)$$

where σ is the mechanical stress tensor. In this description, the constitutive laws that relate the mechanical stress tensor, σ_{ij} , to the mechanical strain tensor, ε_{ij} , define the nature/behavior of the material when subjected to mechanical load. For example, a linearly elastic material assumes that the stress is linearly proportional to the strain. Other models in which stress varies with strain, strain rate, and stress rate are commonly referred to as viscoelastic solids.

With respect to viscoelastic behavior, there have been some recent reports regarding time-dependent behavior of liver tissue when subjected to mechanical loading. Miller [79] extrapolated work performed in brain tissue to data reported by Melvin et al. [76] for the determination of a viscoelastic liver model. Liu and Bilston performed a series of experiments on bovine livers to include oscillation and relaxation tests and generated a five-element Maxwell model [67]. Work by Carter et al. made measurements of in vivo and ex vivo liver specimens in humans and pigs at strain rates consistent with surgical loading. In addition, they developed a nonlinear elastic model to represent their data [17]. Schwartz et al. generated a computational framework to solve a nonlinear viscoelastic model for realistic surgical simulation that was validated using ex vivo liver samples from deer under conditions of perforation from needle biopsy [100]. Rosen et al. conducted a study whereby tissue from seven abdominal organs underwent cyclical and step strain compressions using a motorized endoscopic grasper with the focus of generating realistic viscoelastic haptic tissue models under surgical loading conditions [97].

More recently, sophisticated nonlinear viscoelastic and hyperelastic constitutive models have been proposed as better representations of the stress-strain behavior [39, 114].

While the above represents several examples of constitutive modeling spanning decades, it is important to realize that a clear understanding of the extent of model refinement necessary for effective surgical guidance is continuing to be revealed. More specifically, through observation, we understand the nature of surgical presentation, and the scale of applied surgical manipulations. Through measurement, we understand the accuracy of workflow-amenable digitization equipment as well as image-rendered surgical targets. Only through a comprehensive understanding of these factors can a proper model selection be made. With current state-of-the-art guidance equipment (i.e. optical localizers with measurement accuracies on the order of 0.5 mm and image volumes at the single millimeter resolution) and human-based surgical applicators, the utilization of linear and moderately nonlinear models is likely appropriate for guidance techniques concerned with positional application of surgical tools. With diagnostics, haptic interfaces, or possibly development of robotic manipulators, extension of models may be important.

In the work presented here, we will assume a linear elastic behavior where the stress is linearly proportional to the strain (i.e. Hooke's law) [14]. To solve the resulting system of partial differential equations, many methods are available [63]. The method we have chosen is a standard Galerkin weighted residual approach with linear Lagrange polynomial basis functions [71]. As with many of these types of problems, sparse matrix formats and iterative solvers such as stabilized conjugate gradient with incomplete LU preconditioning are used to solve [15] but many options exist. While model selection will affect fidelity, the design of algorithms to drive correction with sparsely acquired intraoperative data is far more challenging.

3.3.1 Iterative Closest Atlas Technique

Given the organ presentation described above, one strategy to correct for deformation of soft-tissue abdominal organs is to acquire data regarding visible shape change of the organ anterior surface and then extrapolate global organ shape change using computer models. Similar to approaches in non-rigid image registration [98], the framework is initialized via a rigid registration (usually a surface-based registration) with the subsequent application of a non-rigid iterative alignment process to correct for deformations. In previous work, a non-rigid correction was performed using a modified shape atlas technique [29] which we called iterative closest atlas (ICAt) [19, 26]. Figure 10 demonstrates the ICAt framework. The preoperative planning alluded to in Fig. 2 is demonstrated here with sample results (gray region of Fig. 10). Upon completion, the computational model is imported to a finite-element elastic-model solving routine where tens to hundreds of boundary conditions descriptions are employed in an automated fashion to build a comprehensive shape atlas that is representative of typical

surgical deformations. Within the intraoperative environment (red region of Fig. 10), data regarding the exposed organ surface is acquired using a tracked laser range scanner in this case. This data is then rigidly aligned using a salient-feature weighted surface based registration method [26]. Once aligned, the remaining non-rigid effects are compensated for using a regularized least-squares approach which iteratively generates a linear combination of shapes from the shape atlas to best fit the deformations present [27]. While the results were encouraging in realistic phantom conditions, it was found during observations that significant variability in presentation existed such that atlas techniques became challenging. Within the neurosurgical environment, these techniques have been shown to be very powerful [22, 33] and will likely be important as better understanding of deformations due to presentation is improved.

As a result of this difficulty, other strategies have been explored whereby the available sparse data is used to extrapolate deformation boundary conditions to the remainder of the organ. Similar to the previous technique, these approximated boundary conditions are then applied to a finite element biomechanical model of the organ to execute a complete volumetric correction. These strategies are very robust and have demonstrated results that have improved correction although further work is needed. The most significant change in the intraoperative correction framework is shown in Fig. 11 where the steps following the initial alignment have been modified to involved active computer model computations during surgery. Briefly stated, the framework of these methods is to use the initial closest point distance maps (e.g. Fig. 10, colored field in the initial registration) as a means to spatially distribute, i.e. extrapolate, those additional deformation conditions over the remaining surface of the liver thus generating a complete boundary condition set for the computer model. At this time, two strategies have been explored: (1) radial spatial filter and (2) Laplacian PDE filter.

3.3.2 Radial Spatial Filter Method

Two approaches have been attempted and each is an alternate realization of Fig. 11. The first of these methods was presented in [33]. In this approach, the correspondence function between laser range scan data is used to guide the application of boundary conditions similar to work by [19, 20]. However, the difficulty in these direct approaches was that sufficient information regarding posterior surfaces needed to be specified which was difficult to approximate, and flanking regions around the laser range scan partial surface were left unmodified which lead to unnatural looking deformations (i.e. a plug-like effect). In these extrapolation strategies, a spatial surface filter that distributes into the flanking regions of the liver surface is created and more natural deformations are generated. The first approach created radial capture regions that were initially quite large (large enough to propagate to the posterior areas of the liver). These regions served as averaging kernels to distribute the closest-point based boundary condition associated with the sparse intraoperative data from the laser range scanner.

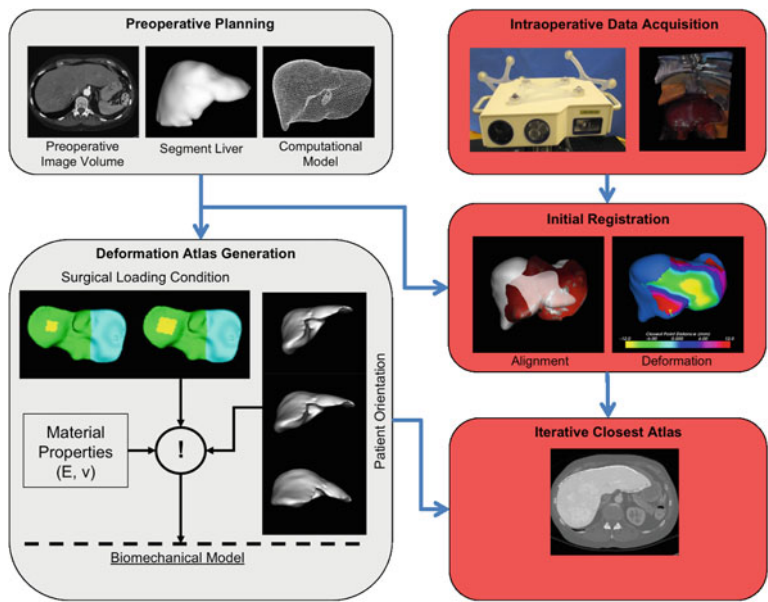


Fig. 10 Iterative closest atlas technique

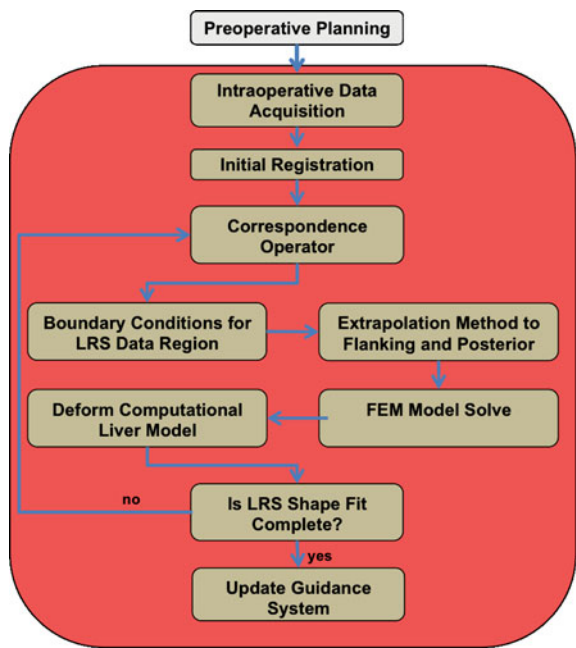


Fig. 11 Active-solve intraoperative local sparse data registration framework that extrapolates data into flanking and posterior regions

With spatially diffuse kernels, the averaging would result in a small increment of deformation to be applied. As kernels are gradually reduced in size, the liver shape would approach that of the laser range scan measurements.

These computations were all compatible with OR timing. It should also be noted that the radial spatial filter was modified by a norm-sensitizer as it distributed boundary conditions to the posterior side of the liver whereby the boundary conditions would change sign to promote more realistic organ movement. One advantage of this filter is that it introduced sufficient boundary conditions such that a priori assumptions regarding the posterior regions of the liver need not be specified rather the filter approach provided sufficient enhancement to the condition number of matrices associated with FEM calculations to allow for rapid robust solutions with standard sparse matrix techniques. While this method was comparable to ICAt, the results were of limited success.

3.3.3 Laplacian PDE Filter Method

From this initial experience, a second method was developed that performed a solution to Laplace's partial differential equation expressed along the organ surface's triangular mesh to extrapolate boundary conditions into the flanking regions. This type of method has been used to assist in non-rigid surface registration of the breast where fiducials were not present [88] and the results were found to be reasonable. Upon completion of the solution of Laplace's equation, the boundary conditions assigned to the posterior regions also underwent the same norm sensitization previously mentioned. Figure 12 demonstrates the result from the both of these intraoperative model computing approaches with all surfaces normalized to the max-min range of displacements. Figure 12 illustrates the results at three different iterations associated with the dynamic radial spatial filter method from our technique reported in [33]. It should be noted that each of the iterations shown represents an increment of displacement (typically about 10–15 applied so the per-increment value is quite small in magnitude). Figure 12 shows the single iteration Laplacian PDE method. The Laplacian method is usually executed as either a single or dual-pass method that makes it considerably faster than the radial method (i.e. only two model solves are necessary versus 10–15 in the radial method).

3.4 Intraoperative Update of Image Guidance System

In Sect. 3.3, the quantitative aspects of deformation correction were described but the problem of integrating deformation into OR work flow was not addressed. In a typical guidance display, the surgeon is presented with orthogonal views of the preoperative medical image volume and a view of the 3D surface model. With deformation comes the necessity to update the guidance display or else the surgeon's virtual display will no longer correspond to their physical reality. If an

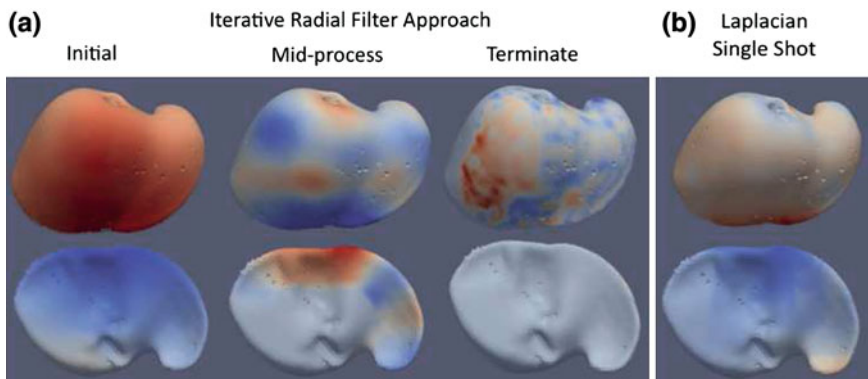


Fig. 12 **a** Initial-mid-and last iteration of boundary condition distribution; **b** single iteration with Laplacian methodology. *Red* indicates displacements applied to model are needed to move along the surface normal while *blue* indicates moving against the surface normal

intraoperative image volume is available, the guidance display could simply be updated with it. The intraoperative volume could even be from a different modality than the preoperative volume (ultrasound mapped to preoperative MRI [43] using thin-plate splines). In the case of deformation correction using mathematical models, there is no intraoperative image for display. Galloway and Peters [38] describe this problem thusly: ‘one of the fundamental concepts of [image-guided interventions], which is that the images represent the present state of the physiology, is only a first approximation’.

A direct method of introducing deformation correction into the guidance system is to apply the volumetric deformation fields to the preoperative images and utilize the deformed images for navigation [78]. Since the liver is the only object for which the volumetric deformation field exists, the position and orientation of non-liver objects within the CT are preserved. This is achieved by initially assigning voxels contained within the liver volumetric mesh to the background intensity in the (new) deformed CT volume. The deformed liver within the deformed CT image volume is created by updating the intensity associated with the deformed position of voxels contained within each element in the volumetric liver mesh. Voxel deformations are interpolated from the nodal deformation field through the use of linear tetrahedral finite-element basis functions, and the intensity of the deformed voxel is computed through trilinear interpolation of the eight nearest neighbor voxels to the original position. The image volume with and without deformation is shown in Fig. 13.

When deforming the image volume, the fine image detail may be lost in this process due to interpolation effects due to low soft-tissue contrast in CT (the imaging modality most often used in liver surgery). To address this deficiency, a novel local stylus transformation was developed which corrects for deformation but also maintains the pristine nature of the images. This method of introducing deformation into the guidance display is to apply the volumetric deformation field

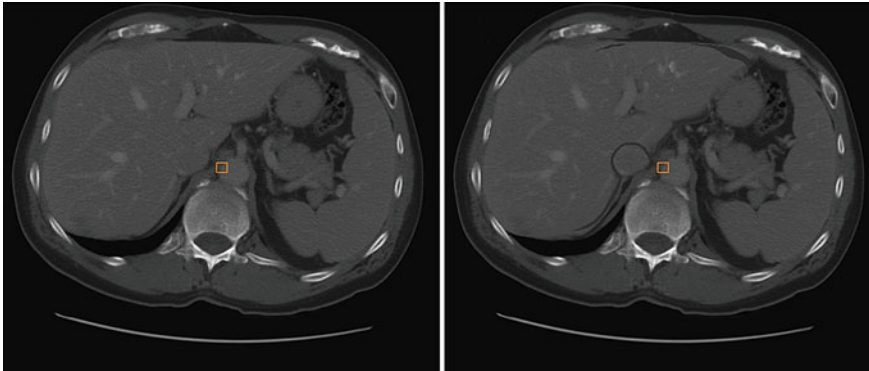


Fig. 13 An axial slice of the undeformed CT volume (*left*) and the corresponding deformed volume (*right*)

to the tip of the surgical tool and leaving the preoperative images *intact*. Typically, in a guidance system, a global rigid registration estimate is applied to each tool tip position. In our deformation corrected method, the global rigid registration is applied followed by a local non-rigid refinement of the transformed tool tip.

More specifically, the global registration rigidly transforms the tool's position from the patient's physical space to the preoperative image space. The non-rigid refinement updates the tool's position on the images using the computed volumetric deformation field. This step requires an interpolation (if the transformed tool position is within the extents defined by the segmented liver) or an extrapolation (if the transformed tool position lies outside of the extents defined by the segmented liver) since the volumetric deformation field does not exist for every point on the preoperative images. The basis functions used in the biomechanical model to compute the volumetric deformation field was used to interpolate the displacement vector at each node in the voxel in the tetrahedral mesh to every voxel the image volume. A simple nearest neighbor approach and a distance-based weighting scheme was used to extrapolate displacements from the tetrahedral mesh to an envelope surrounding the mesh. The guidance display will simply show the updated tool position with the pristine preoperative image volume.

4 Application: Tumor Resection

These methods have been explored using realistic liver phantom experiments. Figure 14 shows the liver phantom centrally located within an arrangement of external fiducials (white spheres). Figure 14 illustrates the CT-rendered results of the phantom in a deformed state. Using this system, a pre-deformation organ configuration was acquired using CT and LRS, and then a series of deformations were applied and the data was acquired again. These data (fiducial points and

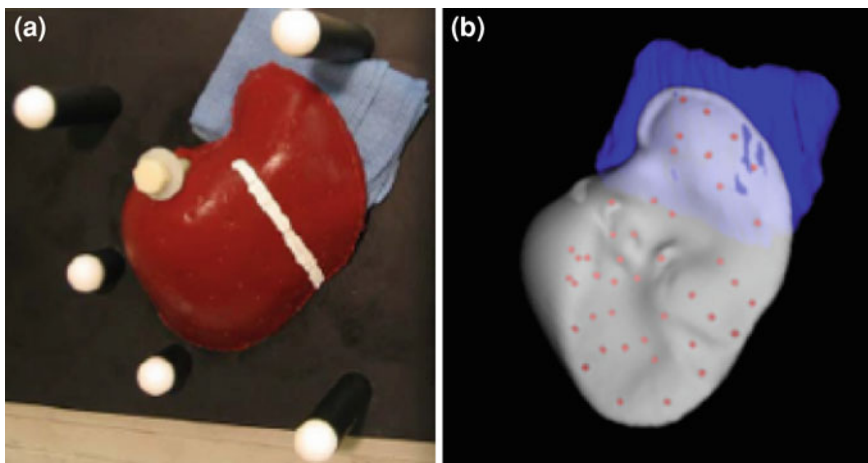


Fig. 14 **a** Liver phantom; **b** CT-rendered surface with applied deformations and bead targets

surfaces) were then used to align the pre-deformation and post-deformation data in a battery of rigid and non-rigid registration algorithms. The targets (shown as beads in Fig. 14) served as novel positions whereby its transformed location could be compared to its CT-acquired counterpart and a TRE could be reported. Table 1 is a comprehensive overview of the results from these experiments.

Looking through the different registrations, it is evident that more data leads to better TRE. We can see that the non-rigid ICAt using sparse data (4th row of results) is approximately equivalent to the data-rich ICP results (3rd row of results—complete organ surfaces available in both states). As we move further down the list, we begin to exceed this result using the radial and then Laplacian PDE method. While this may seem a modest improvement, an appropriate comparison would be to compare the first two rows of results from Table 1 to that of the ICAt and subsequent non-rigid registration methods. These two registration results represent what can realistically be achieved with open abdominal surgery without the use of intraoperative tomographic scanning. When we compare any of the sparse non-rigid registration results (rows 4–7 results) to these, a considerable improvement in targeting error has been achieved. As far as a performance goal, the last row of Table 1 represents what is achievable with a data-rich non-rigid registration environment. If these extrapolative methods can be improved, a surgical platform amenable to the patient workflow associated with abdominal surgery will have been created.

It is clear that more organ surface data would be helpful in designing these methods and while intraoperative CT and MR may be a somewhat intractable solution with respect to surgical workflow, the use of additionally sparse ultrasound data may be an avenue to narrow the gap between sparse and data-rich methods. For example, Fig. 15 illustrates a liver with metastatic lesion and posterior liver surface designated within a preoperative CT liver slice (left) and

Table 1 Results from rigid and non-rigid registration experiment in realistic liver phantom study undergoing deformations

Registration method	Description	Average target error range (mm)	Maximum target error range (mm)
External rigid registration	Fiducials at positions approximately external to abdomen	14.8–22.8	31.0–42.3
Iterative closest point (ICP)	Iterative closest point registration of CT segmented liver surface to intraoperative acquired LRS surface of liver	4.3–4.4	8.8–10.9
Salient feature weighted ICP	Iterative closest point registration of CT segmented liver surface to intraoperative acquired LRS surface of liver with salient features of falciform ligament and inferior ridges	4.1–4.5	10.0–11.3
Surface data-rich ICP	Iterative closest point registration between complete CT segmented liver surface before and after deformation	2.7–3.2	6.7–6.8
ICAt	Iterative closest atlas non-rigid registration using CT segmented liver surface to intraoperative acquired LRS surface of liver	2.5–4.0	5.3–14.3
Radial spatial filter method	Iterative radial spatial filter non-rigid registration using CT segmented liver surface to intraoperative acquired LRS surface of liver	2.6–3.0	8.0–10.5
Laplacian PDE filter method	Surface Laplacian PDE filter non-rigid registration using CT segmented liver surface to intraoperative acquired LRS surface of liver	2.0–2.6	6.4–8.6
Non-rigid	Full surface description with closest-point non-rigid correction	0.6–0.9	1.8–3.3

its approximate corresponding image using intraoperative ultrasound (right). Although the experiments were performed in a liver phantom, Table 1 suggests that additional surface data is the critical step in reducing target error. Utilization of echogenic structures such as the liver posterior surface or the tumor boundary itself may be an important piece of guidance information to further reducing target error.

5 Application: Radio Frequency Ablation

While some tracked intraoperative ultrasound technology approaches have been implemented [61], its widespread integration into guidance platforms is not commonplace. In addition to providing data, tracked intraoperative ultrasound will

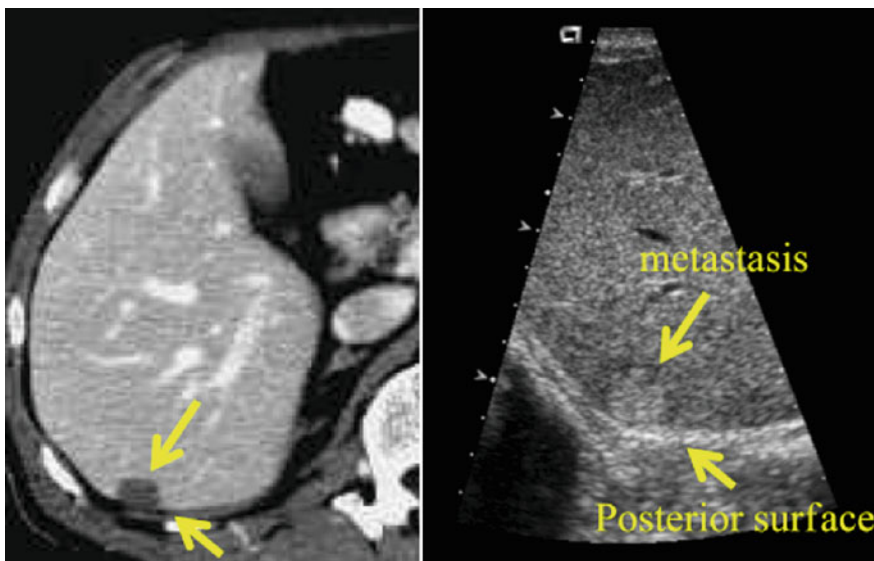


Fig. 15 (left) CT with metastasis and posterior edge of liver, and (right) corresponding objects in ultrasound

likely serve as the best means to validate abdominal image-guidance technologies. Along this direction, to test the potential of correction in the in vivo environment, some preliminary tests have been conducted in two clinical cases at Memorial Sloan-Kettering Cancer Center. In these preliminary tests, the goal was to deliver a radiofrequency ablation (RFA) probe to target (i.e. approximate centroid of tumor). With respect to data, preoperative CT images, an intraoperative swabbed surface of the liver as provided by an optically-tracked stylus, and the final location of the RFA probe in physical space was provided. In placing the RFA probe, the surgeon confirmed the placement of the probe in the centroid used intraoperative ultrasound guidance.

Using this data, the RFA probe tip position was projected using our rigid salient feature registration method (equivalent of row 3 result of Table 1), and then in its model-corrected position (using the Laplacian PDE method of row 7 result of Table 1). Figure 16 shows the first two cases with the model corrected probe position showing clear improvement. With rigid registration, the RF position resided just inside the tumor edge for Case 1 and outside the tumor for Case 2 while the deformation corrected position in both instances placed the probe closer to the tumor centroid which is consistent with the surgeon's procedural experience. While these results are preliminary, it does show promise as a technique as well as the use of ultrasound as a validation tool and quite possibly a potential source for improving the methods.

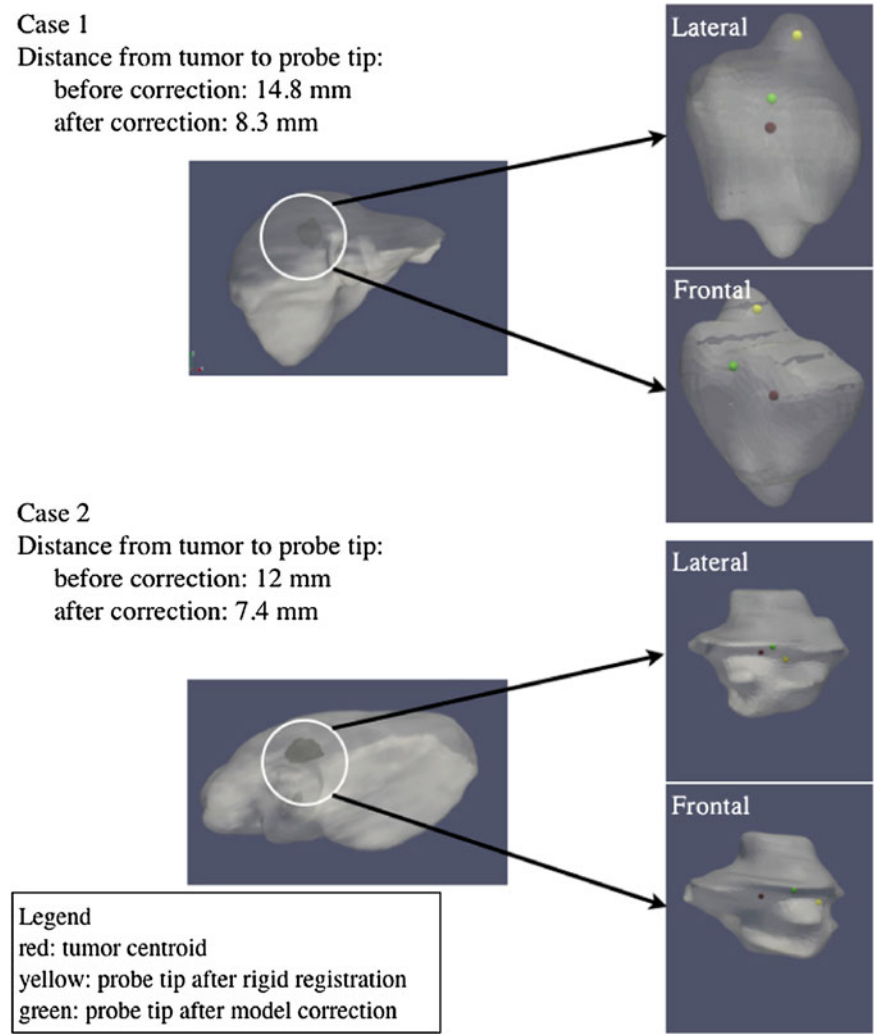


Fig. 16 The RFA probe tip position before and after correction for two clinical cases at Memorial Sloan-Kettering Cancer Center. The distance between the tip before and after correction in relation to 5 mm sphere drawn around the centroid of the tumor improved after correction in both cases

6 Conclusions and Future Directions

While comprehensive data creates the best performance with respect to engineering, if the methods overly encumber the surgeon such that patient care is compromised, these do not represent practical solutions. Each of the methods described above is considerably restricted by the use of sparse data. The final

column in Table 1 emphasizes the importance of comprehensive data. However, the methods reported above have been thoughtfully designed for speed and surgical workflow. In this chapter, it is suggested that computational modeling, sparse data, and constrained extrapolative techniques can sometimes serve as effective alternatives to comprehensive technology solutions. Mathematical modeling has a long history of trying to connect disparate data. Its use here in the surgical domain and in the role of providing enhancement to application of therapeutic processes is an exciting prospect.

Acknowledgments This work is funded by the National Institutes of Health grant R01 CA162477 of the National Cancer Institute. We would like to acknowledge that data was provided by Pathfinder Therapeutics Inc., Nashville, TN and is associated with National Cancer Institute Grant # CA119502. For disclosure, Dr. Miga is a co-founder and holds equity in Pathfinder Therapeutics Inc.

References

1. Ambrosino, G., Polistina, F., Costantin, G., Francescon, P., Guglielmi, R., Zanco, P., Casamassima, F., Febbraro, A., Gerunda, G., Lumachi, F.: Image-guided robotic stereotactic radiosurgery for unresectable liver metastases: preliminary results. *Anticancer Res.* **29**, 3381–3384 (2009)
2. American Cancer Society: Cancer Facts and Figures 2010. American Cancer Society, Atlanta (2010)
3. Archip, N., Clatz, O., Whalen, S., Kacher, D., Fedorov, A., Kot, A., Chrisocholdes, N., Jolesz, F., Golby, A., Black, P.M., Warfield, S.K.: Non-rigid alignment of pre-operative MRI, fMRI, and DT-MRI with intra-operative MRI for enhanced visualization and navigation in image-guided neurosurgery. *NeuroImage* **35**, 609–624 (2007)
4. Audette, M.A., Siddiqi, K., Ferrie, F.P., Peters, T.M.: An integrated range-sensing, segmentation and registration framework for the characterization of intra-surgical brain deformations in image-guided surgery. *Comput. Vis. Image Understand.* **89**, 226–251 (2003)
5. Bao, P., Sinha, T.K., Chen, C.C.R., Warmath, J.R., Galloway, R.L., Herline, A.J.: A prototype ultrasound-guided laparoscopic radiofrequency ablation system. *Surg. Endosc. Other Intervent. Tech.* **21**, 74–79 (2007)
6. Bao, P., Warmath, J., Galloway, R., Herline, A.: Ultrasound-to-computer-tomography registration for image-guided laparoscopic liver surgery. *Surg. Endosc.* **19**, 424–429 (2005)
7. Beller, S., Hnerbein, M., Lange, T., Eulenstein, S., Gebauer, B., Schlag, P.M.: Image-guided surgery of liver metastases by three-dimensional ultrasound-based optoelectronic navigation. *Br. J. Surg.* **94**(7), 866–875 (2007)
8. Besl, P., McKay, N.: A method for registration of 3-D shapes. *IEEE Trans. Pattern Anal. Mach. Intell.* **14**(2), 239–256 (1992)
9. Bismuth, H., Castaing, D., Garden, O.J.: The use of operative ultrasound in surgery of primary liver tumors. *World J. Surg.* **11**, 610–614 (1987)
10. Black, P., Moriarty, T., Alexander, E., Stieg, P., Woodard, E., Gleason, P., Martin, C., Kikinis, R., Schwartz, R., Jolesz, F.: Development and implementation of intraoperative magnetic resonance imaging and its neurosurgical applications. *Neurosurgery* **41**(4), 831–842 (1997)
11. Blackall, J., King, A., Penney, G., Adam, A., Hawkes, D.: A statistical model of respiratory motion and deformation of the liver. In: Niessen, W., Viergever, M. (eds.) *Medical Image*

- Computing and Computer-Assisted Intervention MICCAI 2001. Lecture Notes in Computer Science, vol. 2208, pp. 1338–1340. Springer, Berlin (2001)
12. Blackall, J., Penney, G., King, A., Hawkes, D.: Alignment of sparse freehand 3-D ultrasound with preoperative images of the liver using models of respiratory motion and deformation. *IEEE Trans. Med. Imaging* **24**(11), 1405–1416 (2005)
 13. Blumgart, L.H., Fong, Y.: Surgical options in the treatment of hepatic metastasis from colorectal cancer. *Curr. Probl. Surg.* **32**(5), 333–421 (1995)
 14. Boresi, A.P., Chong, K.P.: *Elasticity in Engineering Mechanics*. 2nd edn. Wiley, New York (2000)
 15. Bramley, R., Wang, X.: SPLIB: a library of iterative methods for sparse linear systems. Technical Report, Department of Computer Science, Indiana University (1997)
 16. Bruns, H., Kratschmer, K., Hinz, U., Brechtel, A., Keller, M., Buchler, M.W., Schemmer, P.: Quality of life after curative liver resection: a single center analysis. *World J. Gastroenterol.* **16**, 2388–2395 (2010)
 17. Carter, F.J., Frank, T.G., Davies, P.J., McLean, D., Cuschieri, A.: Measurements and modelling of the compliance of human and porcine organs. *Med. Image Anal.* **5**, 231–236 (2001)
 18. Carter, T.J., Sermesant, M., Cash, D.M., Barratt, D.C., Tanner, C., Hawkes, D.J.: Application of soft tissue modelling to image-guided surgery. *Med. Eng. Phys.* **27**(10), 893–909 (2005)
 19. Cash, D.M., Miga, M.I., Glasgow, S.C., Dawant, B.M., Clements, L.W., Cao, Z., Galloway, R.L., Chapman, W.C.: Concepts and preliminary data toward the realization of image-guided liver surgery. *J. Gastrointest. Surg.* **11**, 844–859 (2007)
 20. Cash, D.M., Miga, M.I., Sinha, T.K., Galloway, R.L., Chapman, W.C.: Compensating for intra-operative soft tissue deformations using incomplete surface data and finite elements. *IEEE Trans. Med. Imaging* **24**, 1479–1491 (2005)
 21. Cash, D.M., Sinha, T.K., Chapman, W.C., Terawaki, H., Dawant, B.M., Galloway, R.L., Miga, M.I.: Incorporation of a laser range scanner into image-guided liver surgery: surface acquisition, registration, and tracking. *Med. Phys.* **30**, 1671–1682 (2003)
 22. Chen, I., Coffey, A.M., Ding, S.Y., Dumpuri, P., Dawant, B.M., Thompson, R.C., Miga, M.I.: Intraoperative brain shift compensation: accounting for dural septa. *IEEE Trans. Biomed. Eng.* **58**, 499–508 (2011)
 23. Chopra, S., Hnerbein, M., Eulenstein, S., Lange, T., Schlag, P., Beller, S.: Development and validation of a three dimensional ultrasound based navigation system for tumor resection. *Eur. J. Surg. Oncol.* **34**(4), 456–461 (2008)
 24. Chopra, S., Rump, J., Schmidt, S., Streitparth, F., Seebauer, C., Schumacher, G., Van der Voort, I., Teichgraber, U.: Imaging sequences for intraoperative MR-guided laparoscopic liver resection in 1.0-T high field open MRI. *Eur. Radiol.* **19**, 2191–2196 (2009)
 25. Clatz, O., Delingette, H., Talos, I.F., Golby, A.J., Kikinis, R., Jolesz, F.A., Ayache, N., Warfield, S.K.: Robust nonrigid registration to capture brain shift from intraoperative MRI. *IEEE Trans. Med. Imaging* **24**, 1417–1427 (2005)
 26. Clements, L.W., Chapman, W.C., Dawant, B.M., Galloway, R.L., Miga, M.I.: Robust surface registration using salient anatomical features for image-guided liver surgery: algorithm and validation. *Med. Phys.* **35**(6), 2528–2540 (2008)
 27. Clements, L.W., Dumpuri, P., Chapman, R.L., Galloway, R.L., Jr., Miga, M.I.: Atlas-based method for model updating in image-guided liver surgery. In: Cleary, K.R., Miga, M.I. (eds.) *Medical Imaging 2007: Visualization, Image-Guided Procedures, and Modeling*, vol. 6509. SPIE, Nashville (2007)
 28. Conversano, F., Franchini, R., Demitri, C., Massoptier, L., Montagna, F., Maffezzoli, A., Malvasi, A., Casciaro, S.: Hepatic vessel segmentation for 3D planning of liver surgery: experimental evaluation of a new fully automatic algorithm. *Acad. Radiol.* **18**(4), 461–470 (2011)
 29. Davatzikos, C., Shen, D.G., Mohamed, A., Kyriacou, S.K.: A framework for predictive modeling of anatomical deformations. *IEEE Trans. Med. Imaging* **20**, 836–843 (2001)

30. Dawant, B.M., Li, R., Lennon, B., Li, S.: Semi-automatic segmentation of the liver and its evaluation on the MICCAI 2007 grand challenge data set. In: *Proceedings of the MICCAI Workshop on 3-D Segmentation Clinic: A Grand Challenge*, pp. 215–221. Springer, Berlin (2007)
31. DeMatteo, R.P., Palese, C., Jarnagin, W.R., Sun, R.L., Blumgart, L.H., Fong, Y.: Anatomic segmental hepatic resection is superior to wedge resection as an oncologic operation for colorectal liver metastases. *J. Gastrointest. Surg.* **4**(2), 178–184 (2000)
32. DeWitt, J., LeBlanc, J., McHenry, L., Ciaccia, D., Imperiale, T., Chappo, J., Cramer, H., McGreevy, K., Chriswell, M., Sherman, S.: Endoscopic ultrasound-guided fine needle aspiration cytology of solid liver lesions: a large single-center experience. *Am. J. Gastroenterol.* **98**, 1976–1981 (2003)
33. Dumpuri, P., Clements, L.W., Dawant, B.M., Miga, M.I.: Model-updated image-guided liver surgery: preliminary results using surface characterization. *Prog. Biophys. Mol. Biol.* **103**(2–3), 197–207 (2010)
34. Dumpuri, P., Thompson, R.C., Cao, A.Z., Ding, S.Y., Garg, I., Dawant, B.M., Miga, M.I.: A fast and efficient method to compensate for brain shift for tumor resection therapies measured between preoperative and postoperative tomograms. *IEEE Trans. Biomed. Eng.* **57**, 1285–1296 (2010)
35. Fitzpatrick, J.M., West, J.B., Maurer, C.R.: Predicting error in rigid-body point-based registration. *IEEE Trans. Med. Imaging* **17**, 694–702 (1998)
35. Frauenfelder, T., Tutic, M., Weder, W., Gtti, R., Stahel, R., Seifert, B., Opitz, I.: Volumetry: an alternative to assess therapy response for malignant pleural mesothelioma? *Eur. Respir. J.* **38**(1), 162–168 (2011)
37. Frericks, B.B., Caldarone, F.C., Nashan, B., Savellano, D.H., Stamm, G., Kirchhoff, T.D., Shin, H.O., Schenk, A., Selle, D., Spindler, W., Klempnauer, J., Peitgen, H., Galanski, M.: 3D CT modeling of hepatic vessel architecture and volume calculation in living donated liver transplantation. *Eur. Radiol.* **14**, 326–333 (2004)
38. Galloway, R.L., Jr., Peters, T.M.: Overview and history of image-guided interventions. In: Peters, T.M., Cleary, K. (eds.) *Image-Guided Interventions: Technology and Applications*. Springer, Berlin (2008)
39. Gao, Z., Lister, K., Desai, J.P.: Constitutive modeling of liver tissue: experiment and theory. *Ann. Biomed. Eng.* **38**, 505–516 (2010)
40. Garcea, G., Ong, S.L., Maddern, G.J.: Inoperable colorectal liver metastases: a declining entity? *Eur. J. Cancer* **44**, 2555–2572 (2008)
41. Garden, J.O., Bismuth, H.: Anatomy of the liver. In: Carter, D.C. (ed.) *Hepatobiliary and Pancreatic Surgery*, 5th edn., pp. 1–4. Chapman and Hall Medical, London (1996)
42. Glombitza, G., Lamade, W., Demir, A.M., Gopfert, M.R., Mayer, A., Bahner, M.L., Meinzer, H.P., Richter, G., Lehnert, T., Herfarth, C.: Virtual planning of liver resections: image processing, visualization and volumetric evaluation. *Int. J. Med. Inf.* **53**(2–3), 225–237 (1999)
43. Gobbi, D., Comeau, R., Peters, T.: Ultrasound/MRI overlay with image warping for neurosurgery. In: Delp, S., DiGoia, A., Jaramaz, B. (eds.) *Medical Image Computing and Computer-Assisted Intervention MICCAI 2000. Lecture Notes in Computer Science*, vol. 1935, pp. 29–53. Springer, Berlin (2000)
44. Guimaraes, C.M., Correia, M.M., Baldisserotto, M., de Queiroz Aires, E.P., Coelho, J.F.: Intraoperative ultrasonography of the liver in patients with abdominal tumors: a new approach. *J. Ultrasound Med.* **23**(12), 1549–1555 (2004)
45. Hansen, C., Wiefelich, J., Ritter, F., Rieder, C., Peitgen, H.O.: Illustrative visualization of 3D planning models for augmented reality in liver surgery. *Int. J. Comput. Assist. Radiol. Surg.* **5**, 133–141 (2010)
46. Hartov, A., Roberts, D.W., Paulsen, K.D.: A comparative analysis of coregistered ultrasound and magnetic resonance imaging in neurosurgery. *Neurosurgery* **62**, 91–99 (2008)

47. Heizmann, O., Zidowitz, S., Bourquain, H., Potthast, S., Peitgen, H.O., Oertli, D., Kettelhack, C.: Assessment of intraoperative liver deformation during hepatic resection: prospective clinical study. *World J. Surg.* **34**, 1887–1893 (2010)
48. Herline, A.J., Stefansic, J.D., Debelak, J.P., Hartmann, S.L., Pinson, C.W., Galloway, R.L., Chapman, W.C.: Image-guided surgery: preliminary feasibility studies of frameless stereotactic liver surgery. *Arch. Surg.* **134**(6), 644–650 (1999)
49. Hermoye, L., Laamari-Azjal, I., Cao, Z.J., Annet, L., Lerut, J., Dawant, B.M., Beers, B.E.V.: Liver segmentation in living liver transplant donors: comparison of semiautomatic and manual methods. *Radiology* **234**, 171–178 (2005)
50. Ito, K., Govindarajan, A., Ito, H., Fong, Y.: Surgical treatment of hepatic colorectal metastasis evolving role in the setting of improving systemic therapies and ablative treatments in the 21st century. *Cancer J.* **16**, 103–110 (2010)
51. Jarnagin, W.R., Gonen, M., Fong, Y., DeMatteo, R.P., Ben-Porat, L., Little, S., Corvera, C., Weber, S., Blumgart, L.: Improvement in perioperative outcome after hepatic resection: analysis of 1803 consecutive cases over the past decade. *Ann. Surg.* **236**, 397–406 (2002)
52. Je, H., Choi, E., Ahn, S., Lee, S., Park, S., Kim, J.: Analysis of respiratory induced liver motion using fiducial marker in stereotactic radiosurgery for liver tumor. *Int. J. Radiat. Oncol. Biol. Phys.* **72**, S543 (2008)
53. Ji, S.B., Wu, Z.J., Hartov, A., Roberts, D.W., Paulsen, K.D.: Mutual-information-based image to patient re-registration using intraoperative ultrasound in image-guided neurosurgery. *Med. Phys.* **35**, 4612–4624 (2008)
54. Kleemann, M., Hildebrand, P., BIRTH, M., Bruch, H.: Laparoscopic ultrasound navigation in liver surgery: technical aspects and accuracy. *Surg. Endosc.* **20**, 726–729 (2006)
55. Kopetz, S., Chang, G.J., Overman, M.J., Eng, C., Sargent, D.J., Larson, D.W., Grothey, A., Vauthey, J.N., Nagorney, D.M., McWilliams, R.R.: Improved survival in metastatic colorectal cancer is associated with adoption of hepatic resection and improved chemotherapy. *J. Clin. Oncol.* **27**, 3677–3683 (2009)
56. Lamade, W., Glombitza, G., Fischer, L., Chiu, P., Cardenas, C.E., Sr., Thorn, M., Meinzer, H.P., Grenacher, L., Bauer, H., Lehnert, T., Herfarth, C.: The impact of 3-dimensional reconstructions on operation planning in liver surgery. *Arch. Surg.* **135**(11), 1256–1261 (2000)
57. Lamata, P., Lamata, F., Sojar, V., Makowski, P., Massoptier, L., Casciaro, S., Ali, W., Stüdeli, T., Declerck, J., Elle, O., Edwin, B.: Use of the resection map system as guidance during hepatectomy. *Surg. Endosc.* **24**, 2327–2337 (2010)
58. Lang, H., Radtke, A., Hindennach, M., Schroeder, T., Fruhauf, N.R., Malago, M., Bourquain, H., Peitgen, H.O., Oldhafer, K.J., Broelsch, C.E.: Impact of virtual tumor resection and computer-assisted risk analysis on operation planning and intraoperative strategy in major hepatic resection. *Arch. Surg.* **140**(7), 629–638 (2005)
59. Lang, H., Radtke, A., Liu, C., Frhauf, N.R., Peitgen, H.O., Broelsch, C.E.: Extended left hepatectomy modified operation planning based on three-dimensional visualization of liver anatomy. *Langenbecks Arch. Surg.* **389**, 306–310 (2004)
60. Lange, T., Eulenstein, S., Hunerbein, M., Lamecker, H., Schlag, P.M.: Augmenting intraoperative 3D ultrasound with preoperative models for navigation in liver surgery. In: Barillot, C., Haynor, D., Hellier, P. (eds.) *Medical Image Computing and Computer-Assisted Intervention MICCAI 2004. Lecture Notes in Computer Science*, vol. 3217, pp. 534–541. Springer, Berlin (2004)
61. Lange, T., Papenberg, N., Heldmann, S., Modersitzki, J., Fischer, B., Lamecker, H., Schlag, P.: 3D ultrasound-CT registration of the liver using combined landmark-intensity information. *Int. J. Comput. Assist. Radiol. Surg.* **4**, 79–88 (2009)
62. Lange, T., Wenckebach, T.H., Lamecker, H., Seebass, M., Hunerbein, M., Eulenstein, S., Gebauer, B., Schlag, P.M.: Registration of different phases of contrast-enhanced CT/MRI data for computer-assisted liver surgery planning: evaluation of state-of-the-art methods. *Int. J. Med. Robotics Comput. Assist. Surg.* **1**, 6–20 (2005)

63. Lapidus, L., Pinder, G.F.: Numerical Solution of Partial Differential Equations in Science and Engineering. Wiley, New York (1982)
64. Lathrop, R.A., Hackworth, D.M., Webster, R.J.: Minimally invasive holographic surface scanning for soft-tissue image registration. *IEEE Trans. Biomed. Eng.* **57**(6), 1497–1506 (2010)
65. Laurent, C., Sa Cunha, A., Couderc, P., Rullier, E., Saric, J.: Influence of postoperative morbidity on long-term survival following liver resection for colorectal metastases. *Br. J. Surg.* **90**(9), 1131–1136 (2003)
66. Li, S., Waite, J., Lennon, B., Li, R., Dawant, B., Stefansic, J.: Development of preoperative liver and vascular system segmentation and modeling tool for image-guided surgery and surgical planning. In: Cleary, K.R. Miga, M.I. (eds.) *Medical Imaging 2008: Visualization, Image-Guided Procedures, and Modeling*, vol. 6918. SPIE, , San Diego (2008)
67. Liu, Z., Bilston, L.: On the viscoelastic character of liver tissue: experiments and modelling of the linear behaviour. *Biorheology* **37**, 191–201 (2000)
68. Lorensen, W.E., Cline, H.E.: Marching cubes: a high resolution 3D surface construction algorithm. In: *Proceedings of the 14th Annual Conference on Computer Graphics and Interactive Techniques, SIGGRAPH '87*, pp. 163–169. ACM, New York (1987)
69. Lu, Q., Luo, Y., Yuan, C.X., Zeng, Y., Wu, H., Lei, Z., Zhong, Y., Fan, Y.T., Wang, H.H.: Value of contrast-enhanced intraoperative ultrasound for cirrhotic patients with hepatocellular carcinoma: a report of 20 cases. *World J. Gastroenterol.* **14**, 4005–4010 (2008)
70. Lunn, K.E., Paulsen, K.D., Liu, F.H., Kennedy, F.E., Hartov, A., Roberts, D.W.: Data-guided brain deformation modeling: evaluation of a 3-D adjoint inversion method in porcine studies. *IEEE Trans. Biomed. Eng.* **53**, 1893–1900 (2006)
71. Lynch, D.R.: *Numerical Partial Differential Equations for Environmental Scientists and Engineers*. Springer, New York (2005)
72. Ma, B., Ellis, R.E.: Robust registration for computer-integrated orthopedic surgery: laboratory validation and clinical experience. *Med. Image Anal.* **7**(3), 237–250 (2003)
73. Martin, R., Husheck, S., Scoggins, C., McMasters, K.: Intraoperative magnetic resonance imaging for ablation of hepatic tumors. *Surg. Endosc.* **20**, 1536–1542 (2006)
74. Martin, R.C.: Intraoperative magnetic resonance imaging ablation of hepatic tumors. *Am. J. Surg.* **189**, 388–394 (2005)
75. Maurer, C.R., Hill, D.L.G., Maciunas, R.J., Barwise, J.A., Fitzpatrick, J.M., Wang, M.: Measurement of intraoperative brain surface deformation under a craniotomy. In: Wells, W., Colchester, A., Delp, S. (eds.) *Medical Image Computing and Computer-Assisted Intervention MICCAI98. Lecture Notes in Computer Science*, vol. 1496, pp. 51–62. Springer, Berlin (1998)
76. Melvin, J.W., Stalnaker, R.L., Roberts, V.L., Trollope, M.L.: Impact injury mechanisms in abdominal organs. *SAE Trans.* **730968**, 115–126 (1973)
77. Miga, M.I., Dumpuri, P., Simpson, A.L., Weis, J.A., Jarnagin, W.R.: The sparse data extrapolation problem: strategies for soft-tissue correction for image-guided liver surgery. In: Wong, K.H., Holmes, D.R., III (eds.) *Medical Imaging 2011: Visualization, Image-Guided Procedures, and Modeling*, vol. 7964. SPIE, San Diego (2011)
78. Miga, M.I., Roberts, D.W., Kennedy, F.E., Platenik, L.A., Hartov, A., Lunn, K.E., Paulsen, K.D.: Modeling of retraction and resection for intraoperative updating of images during surgery. *Neurosurgery* **49**, 75–85 (2001)
79. Miller, K.: Constitutive modelling of abdominal organs. *J. Biomech.* **33**, 367–373 (2000)
80. Moche, M., Schmitgen, A., Schneider, J.P., Bublat, M., Schulz, T., Voerke, C., Trantakis, C., Bennek, J., Kahn, T., Busse, H.: First clinical experience with extended planning and navigation in an interventional MRI unit. *Rofo-Fortschritte Auf Dem Gebiet Der Rontgenstrahlen Und Der Bildgebenden Verfahren* **176**, 1013–1020 (2004)
81. Nakamoto, M., Hirayama, H., Sato, Y., Konishi, K., Kakeji, Y., Hashizume, M., Tamura, S.: Recovery of respiratory motion and deformation of the liver using laparoscopic freehand 3D ultrasound system. *Med. Image Anal.* **11**(5), 429–442 (2007)

82. Nakamoto, M., Sato, Y., Miyamoto, M., Nakamjima, Y., Konishi, K., Shimada, M., Hashizume, M., Tamura, S.: 3D ultrasound system using a magneto-optic hybrid tracker for augmented reality visualization in laparoscopic liver surgery. In: Dohi, T., Kikinis, R. (eds.) *Medical Image Computing and Computer-Assisted Intervention MICCAI 2002. Lecture Notes in Computer Science*, vol. 2489, pp. 148–155. Springer, Berlin (2002)
83. Nicolau, S., Pennec, X., Soler, L., Buy, X., Gangi, A., Ayache, N., Marescaux, J.: An augmented reality system for liver thermal ablation: design and evaluation on clinical cases. *Med. Image Anal.* **13**(3), 494–506 (2009)
84. Nikfarjam, M., Shereef, S., Kimchi, E., Gusani, N., Jiang, Y., Avella, D., Mahraj, R., Staveley-OCarroll, K.: Survival outcomes of patients with colorectal liver metastases following hepatic resection or ablation in the era of effective chemotherapy. *Ann. Surg. Oncol.* **16**, 1860–1867 (2009)
85. Nimsky, C., Ganslandt, O., Cerny, S., Hastreiter, P., Greiner, G., Fahlbusch, R.: Quantification of, visualization of, and compensation for brain shift using intraoperative magnetic resonance imaging. *Neurosurgery* **47**(5), 1070–1079 (2000)
86. Norero, E., Jarufe, N., Butte, J.M., Norero, B., Duarte, I., Torres, J., Pinedo, G., Lopez, F., Guerra, J.F., Ibanez, L., Zuniga, A., Guzman, S., Martinez, J.: Outcome of surgical treatment of liver metastases from colorectal cancer. *Rev. Med. Chile* **137**, 487–496 (2009)
87. Nougaret, S., Jung, B., Aufort, S., Chanques, G., Jaber, S., Gallix, B.: Adrenal gland volume measurement in septic shock and control patients: a pilot study. *Eur. Radiol.* **20**, 2348–2357 (2010)
88. Ong, R.E., Ou, J.J., Miga, M.I.: Non-rigid registration of breast surfaces using the Laplace and diffusion equations. *Biomed. Eng. Online* **9**, 2 (2010)
89. Patriciu, A., Awad, M., Solomon, S., Choti, M., Mazilu, D., Kavoussi, L., Stoianovici, D.: Robotic assisted radio-frequency ablation of liver tumors randomized patient study. In: Duncan, J., Gerig, G. (eds.) *Medical Image Computing and Computer-Assisted Intervention MICCAI 2005. Lecture Notes in Computer Science*, vol. 3750, pp. 526–533. Springer, Berlin (2005)
90. Penney, G., Blackall, J., Hamady, M., Sabharwal, T., Adam, A., Hawkes, D.: Registration of freehand 3D ultrasound and magnetic resonance liver images. *Med. Image Anal.* **8**(1), 81–91 (2004)
91. Peterhans, M., vom Berg, A., Dagon, B., Inderbitzin, D., Baur, C., Candinas, D., Weber, S.: A navigation system for open liver surgery: design, workflow and first clinical applications. *Int. J. Med. Robotics Comput. Assist. Surg.* **7**(1), 7–16 (2011)
92. Petrowsky, H., Breitenstein, S., Slankamenac, K., Vetter, D., Lehmann, K., Heinrich, S., DeOliveira, M.L., Jochum, W., Weishaupt, D., Frauenfelder, T., et al.: Effects of pentoxifylline on liver regeneration: a double-blinded, randomized, controlled trial in 101 patients undergoing major liver resection. *Annals of Surgery* **252**(5), 813–822 (2010)
93. Pheiffer, T.S., Lennon, B., Simpson, A.L., Miga, M.I.: Development of a novel laser range scanner. In: Wong, K.H., Holmes, D.R., III (eds.) *Medical Imaging 2011: Visualization, Image-Guided Procedures, and Modeling*, vol. 7964. SPIE, San Diego (2011)
94. Pianka, F., Baumhauer, M., Stein, D., Radeleff, B., Schmied, B., Meinzer, H.P., Miller, S.: Liver tissue sparing resection using a novel planning tool. *Langenbecks Arch. Surg.* **396**, 201–208 (2011)
95. Pua, E., Fronheiser, M., Noble, J., Light, E., Wolf, P., von Allmen, D., Smith, S.: 3-D ultrasound guidance of surgical robotics: a feasibility study. *IEEE Trans. Ultrason. Ferroelectr. Freq. Control* **53**(11), 1999–2008 (2006)
96. Risholm, P., Golby, A.J., Wells, W.: Multimodal image registration for preoperative planning and image-guided neurosurgical procedures. *Neurosurg. Clin. N. Am.* **22**, 197–206 (2011)
97. Rosen, J., Brown, J.D., De, S., Sinanan, M., Hannaford, B.: Biomechanical properties of abdominal organs in vivo and postmortem under compression loads. *J. Biomech. Eng.* **130**, 021020-1–021020-17 (2008)

98. Rueckert, D., Sonoda, L.I., Hayes, C., Hill, D.L.G., Leach, M.O., Hawkes, D.J.: Nonrigid registration using free-form deformations: application to breast MR images. *IEEE Trans. Med. Imaging* **18**, 712–721 (1999)
99. Schindl, M.J., Redhead, D.N., Fearon, K.C.H., Garden, O.J., Wigmore, S.J.: The value of residual liver volume as a predictor of hepatic dysfunction and infection after major liver resection. *Gut* **54**, 289–296 (2005)
100. Schwartz, J.M., Denninger, M., Rancourt, D., Moisan, C., Laurendeau, D.: Modelling liver tissue properties using a non-linear visco-elastic model for surgery simulation. *Med. Image Anal.* **9**, 103–112 (2005)
101. Selle, D., Preim, B., Schenk, A., Peitgen, H.: Analysis of vasculature for liver surgical planning. *IEEE Trans. Med. Imaging* **21**(11), 1344–1357 (2002)
102. Sinha, T.K., Dawant, B.M., Duay, V., Cash, D.M., Weil, R.J., Thompson, R.C., Weaver, K.D., Miga, M.I.: A method to track cortical surface deformations using a laser range scanner. *IEEE Trans. Med. Imaging* **24**(6), 767–781 (2005)
103. Sirat, G., Psaltis, D.: Conoscopic holography. *Optics Lett.* **10**(1), 4–6 (1985)
104. Stintzing, S., Hoffmann, R.T., Heinemann, V., Kufeld, M., Rentsch, M., Muacevic, A.: Radiosurgery of liver tumors: value of robotic radiosurgical device to treat liver tumors. *Ann. Surg. Oncol.* **17**, 2877–2883 (2010)
105. Sullivan, J.M., Charron, G., Paulsen, K.D.: A three-dimensional mesh generator for arbitrary multiple material domains. *Finite Elem. Anal. Des.* **25**(3–4), 219–241 (1997)
106. Sun, H., Lunn, K.E., Farid, H., Wu, Z.J., Roberts, D.W., Hartov, A., Paulsen, K.D.: Stereopsis-guided brain shift compensation. *IEEE Trans. Med. Imaging* **24**, 1039–1052 (2005)
107. Suthau, T., Vetter, M., Hassenpflug, P., Meinzer, H.P., Hellwich, O.: A concept work for augmented reality visualization based on a medical application in liver surgery. In: *Proceedings of the ISPRS Commission V Symposium*, pp. 274–280 (2002)
108. Torzilli, G., Botea, F., Procopio, F., Donadon, M., Balzarini, L., Lutman, F., Calliada, F., Montorsi, M.: Use of contrast-enhanced intraoperative ultrasonography during liver surgery for colorectal cancer liver metastases—its impact on operative outcome: analysis of a prospective cohort study. *Eur. J. Cancer Suppl.* **6**(11), 16–23 (2008)
109. Valdes, P.A., Fan, X.Y., Ji, S.B., Harris, B.T., Paulsen, K.D., Roberts, D.W.: Estimation of brain deformation for volumetric image updating in protoporphyrin IX fluorescence-guided resection. *Stereot. Funct. Neurosurg.* **88**, 1–10 (2010)
110. Vigneron, L.M., Warfield, S.K., Robe, P.A., Verly, J.G.: 3D XFEM-based modeling of retraction for preoperative image update. *Comput. Aided Surg.* **16**, 121–134 (2011)
111. Widmann, G., Schullian, P., Haidu, M., Wiedermann, F.J., Bale, R.: Respiratory motion control for stereotactic and robotic liver interventions. *Int. J. Med. Robotics Comput. Assist. Surg.* **6**(3), 343–349 (2010)
112. Wolf, I., van Rikxoort, E., Raicu, D.S., Rau, A.M., Nemeth, G., Meinzer, H., Li, S., Li, R., Lennon, B., Lee, J., Lange, T., Lamecker, H., Rousson, M., Rusko, L., Wimmer, A., Waite, J., Susomboon, R., Soza, G., Sorantin, E., Slagmolen, P., Shimizu, A., Seghers, D., Schmidt, G., Saddi, K., Kobatake, H., Kitney, R., Kainmueller, D., Bello, F., Bekes, G., Beichel, R., Becker, C., Beck, A., Bauer, C., Aurich, V., Arzhaeva, Y., Styner, M., van Ginneken, B., Binnig, G., Bischof, H., Hornegger, J., Grenacher, L., Furukawa, D., Furst, J., Fidrich, M., Dawant, B., Cordova, A., Chi, Y., Cashman, P., Bornik, A., Heimann, T.: Comparison and evaluation of methods for liver segmentation from CT datasets. *IEEE Trans. Med. Imaging* **28**(8), 1251–1265 (2009)
113. Yang, J.D., Roberts, L.R.: Hepatocellular carcinoma: a global view. *Nat. Rev. Gastroenterol. Hepatol.* **7**, 448–458 (2010)
114. Zhong, H., Peters, T.: A real time hyperelastic tissue model. *Comput. Methods Biomech. Biomed. Eng.* **10**, 185–193 (2007)

<http://www.springer.com/978-3-642-29013-8>

Soft Tissue Biomechanical Modeling for Computer
Assisted Surgery

Payan, Y. (Ed.)

2012, X, 398 p., Hardcover

ISBN: 978-3-642-29013-8